AIAA JOURNAL
Vol. 41, No. 5, May 2003

Influence of Contact Phenomena on Embedded Delaminations Growth in Composites

Aniello Riccio*
Centro Italiano Ricerche Aerospaziali, 81043 Capua, Italy
Francesco Scaramuzzino†
Seconda Università degli Studi di Napoli, 81031 Aversa, Italy
and
Pierluigi Perugini*
Centro Italiano Ricerche Aerospaziali, 81043 Capua, Italy

Numerical geometrically nonlinear analyses have been performed to investigate the influence of contact phenomena on multiple embedded delamination growth in composite panels under compressive load. An in-house finite element method code based on the modified virtual crack closure technique, which analyses delamination growth, combined with the penalty method approach, which takes into account contact phenomena, was used for computations. Compressed composite panels with two embedded delaminations have been investigated for various geometrical configurations with different delaminations' sizes and positions. Comparisons with a single embedded delamination model introduced in previous papers are presented. Finally a comparison between contact and no-contact approaches is shown for a significant geometrical configuration.

I. Introduction

THE high specific strength and stiffness of laminated composites make them suitable for use in aircraft structures. However, the high sensitivity of composites to the presence of delaminations, arising after impact with foreign objects or caused by manufacturing defects, has been observed in experimental tests. The lack of robust models for predicting the damage tolerance of composite structures has led to overconservative designs, not fully realizing the promised economical benefits. So it is necessary to produce much more information on these kinds of structures, taking into account the effects of delaminations and their evolution. This should be done introducing new numerical models representing phenomena governing structural behavior of composites such as contact between delaminated plies and delamination growth.

The through-the-width delaminations have been investigated using a great number of analytical and numerical models[1–3] and with the aid of experimental tests.[4–6] Embedded delaminations have also been studied. In literature analytical models,[7–10] experimental tests[11,12] and numerical models[13–19] are presented. In Refs. 13 and 14 numerical analyses have been carried out to study the influence of the geometrical parameters of the embedded delaminations on the buckling modes of composite panels, whereas in Refs. 15 and 16 the influence of contact phenomena on the strain energy release rate distribution along the embedded delaminations front has been widely investigated for composite panels with single delaminations. A mechanical model for the problem of unilaterally constrained, finite, rectangular plates is presented in Ref. 17, such a model is adopted in Ref. 18 to point out the importance of contact phenomena for the correct simulation of the buckling phenomenon in delaminated composite plates. However, none of the papers just mentioned has introduced models to simulate growth of delaminations. On the contrary, in Ref. 19 a detailed investigation on embedded delamination growth has been carried out, but only panels with single delaminations have been investigated without giving information on the contributions of single opening crack modes on the total strain energy release rate. Delamination buckling, postbuckling, and growth are simulated in Ref. 20 by means of an unified approach based on an interface decohesion law; applications of this approach to plates containing delaminations with different shapes and differently positioned along the thickness are also presented.

We wrote the present paper as a natural extension of previous works about the study of stable through-the-width delamination growth,[21] unstable through-the-width delamination growth,[22] and single embedded delamination growth.[23,24] The numerical approach described and validated in Refs. 23 and 24 has been used here to analyze the compressive behavior of composite panels with multiple embedded delaminations.

In Sec. II the adopted finite element approach is presented. In Sec. III a numerical investigation on contact phenomena and delamination growth in compressed composite panels with two embedded delaminations is introduced. Various geometrical configurations with different delaminations' sizes and positions are investigated. Comparisons with the results obtained for the single embedded delamination model used in Ref. 24 are also shown. Finally a comparison between contact and no-contact approaches for a particular geometrical configuration is presented. This comparison points out the influence of contact phenomena on embedded delamination growth and on the whole compressive behavior of delaminated composite panels.

II. Finite Element Approach

Numerical analyses have been performed using the nonlinear finite element code B2000 (Ref. 25). The code is based on total Lagrangian formulation. The incremental continuation method by Riks[26] is adopted to solve the nonlinear equilibrium equations. To perform the numerical analyses for predicting the delamination growth, the B2000 features have been enhanced by means of 1) modifications to continuation method, 2) introduction of a contact element, and 3) introduction of an interface fracture element. The modifications-to-continuation method have been carried out to simulate unstable crack growth; further details on them can be found in Ref. 23. The next two subsections describe the main characteristics of new elements introduced in B2000.

A. Contact Element

Depending on delaminations' geometrical parameters and laminate stacking sequences, contacts can occur somewhere in the

Received 13 January 2001; revision received 20 September 2001; accepted for publication 9 December 2002.

*Researcher, Via Maiorise.
†Professor, Department of Aerospace Engineering, Via Roma 29.

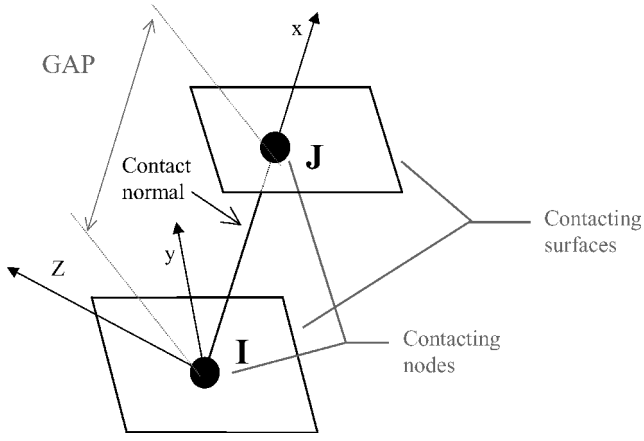

Fig. 1 Three-dimensional node-to-node contact element.

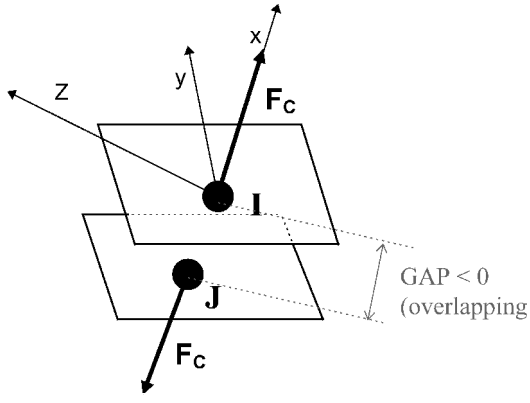

Fig. 2 Three-dimensional node-to-node contact element (contact condition).

delaminated regions. To prevent interpenetrations between the two contacting surfaces, contact forces should be taken into account during analyses. So a three-dimensional node-to-node contact element (shown in Fig. 1) has been introduced in our finite element method (FEM) code. This element is based on the penalty method because of its minimum requirements in terms of computational cost. In the penalty formulation, when contact occurs (Fig. 2), a little overlapping ($GAP < 0$) between the two contacting nodes is allowed, and the contact force F_C acting between these nodes is found as a linear function of their overlapping, according to the following expression:

$$|F_c| = \alpha \cdot |GAP| \tag{1}$$

where α is the penalty constant. Equation (1) shows up the strong dependence of the overlapping (GAP) from the penalty constant. The major weak point of penalty method is just related to the choice of α: too low values of α allow big overlapping, whereas too high values of α can cause convergence problems in the solution of the nonlinear equilibrium equations. In addiction it should be noted that, because of its simplified and saving CPU cost-oriented formulation, the use of node-point-to-node-point approach should be limited to the contact regions not subjected to strong changes in the contact normal. The preceding consideration points out the high degree of experience needed in the selection of regions suitable for node-to-node approach and in the choice of penalty constant to perform effective analyses with the proposed contact element.

B. Fracture Element

From fracture mechanics of composites, it is well known that strain energy release rate rules the propagation of cracks. For each fracture mode (opening mode I, forward shear mode II, and parallel shear mode III) a strain energy release rate can be defined: G_{I} for mode I, G_{II} for mode II, and G_{III} for mode III.

Once known, from ad hoc experiments the crack propagation values for the basic fracture modes (G_{IC}, G_{IIC} and G_{IIIC}), it is possible to predict mixed modes crack propagations in laminates by means of suitable criteria such as the power law criterion:

$$\left(G_{\mathrm{I}}/G_{\mathrm{I}_C}\right)^{\alpha} + \left(G_{\mathrm{II}}/G_{\mathrm{II}_C}\right)^{\beta} + \left(G_{\mathrm{III}}/G_{\mathrm{III}_C}\right)^{\gamma} = E_d \geq 1 \tag{2}$$

In our calculations α, β, and γ have been assumed to be $= 1$ (linear criterion). The satisfaction of relation (2) is assumed to be the necessary condition for crack propagation.

The delamination growth model was implemented in our finite element code by means of a new nine-noded interface fracture element. This element uses the modified virtual crack closure technique (MVCCT) presented in Ref. 27 to calculate the strain energy release rate along the delamination front. The standard VCCT is based on the consideration that the strain energy released by a crack growing from length a to $a + \Delta a$ is equal to the amount of the work required to close the same crack from $a + \Delta a$ to a. So the implementation of such a method allows us to calculate the strain energy released by a crack as a crack closure work, but it involves two analyses, one with the current crack front and the other with the crack front appropriately extended. On the contrary, the MVCCT, based on the $\Delta a/a \ll 1$ hypothesis, assumes that the crack front does not undergo substantial changes in the passage from the crack length a to $a + \Delta a$; so the second step calculations (with extended crack configuration) can be avoided, and it is possible to compute the energy release rate (ERR) contributions in one step using nodal forces and displacements estimated at the actual crack front.

The interface fracture elements are placed between the solid elements with the nodes rigidly connected to the nodes of the adjacent solid elements. The unit virtual crack closure work (= strain energy release rate) for each fracture mode is computed using nodal forces and nodal displacements estimated at the delamination front. For example, the energy release rates associated to the interface fracture element shown in Fig. 3 are

$$G_{\mathrm{I}}^{H} = \tfrac{1}{2} \cdot 1/[(A_1 + A_2)/2] \cdot F_n^H \cdot \left(u_n^M - u_n^L\right)$$

$$G_{\mathrm{II}}^{H} = \tfrac{1}{2} \cdot 1/[(A_1 + A_2)/2] \cdot F_t^H \cdot \left(u_t^M - u_t^L\right)$$

$$G_{\mathrm{III}}^{H} = \tfrac{1}{2} \cdot 1/[(A_1 + A_2)/2] \cdot F_s^H \cdot \left(u_s^M - u_s^L\right) \tag{3}$$

Also contact capabilities, based on the penalty method, are implemented in the interface fracture element to take into account the contact phenomena that can occur between the delaminated regions where delaminations growth. The interface fracture element local coordinate system (t, s, n), shown in Fig. 3a, is used to take into account the large rotations of the delamination front for the calculation of fracture modes contributions and contact forces during growth. Introducing the computed values of G_{I}, G_{II}, and G_{III} in relation (2), it is possible to check whether the propagation occurs. For the interface fracture element of Fig. 3, the satisfaction of relation (2) leads to the release of the node H (Fig. 3b) that causes a modification in the delamination front.

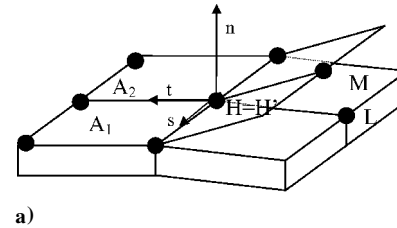

a)

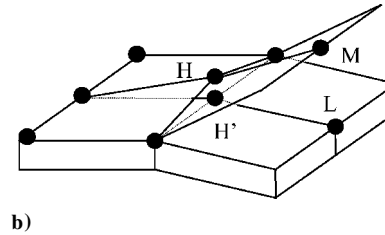

b)

Fig. 3 Interface fracture element.

III. Numerical Results for Composite Panels with Two Embedded Delaminations

A. Parametric Study

The developed numerical tool, whose effectiveness was extensively tested against experimental results,[23] has been adopted to perform a limited parametric analysis. To investigate the influence of contact phenomena, delamination, growth and delaminations' interactions on the compressive behavior of composite panels, a cross-ply laminate $[90\ \text{deg}/0\ \text{deg}/90\ \text{deg}]_{16}$, containing two embedded circular delaminations and undergoing compressive load, has been selected to perform our numerical analysis. The panels' material and geometrical characteristics, shown in Tables 1 and 2 and in Fig. 4, have been chosen in order to highlight the phenomena under consideration. Delaminations' size and delaminations' position along the thickness have been considered as parameters. Four cases with different combinations of delamination diameters (D_1, D_2) and delaminations' abscissa along the thickness (h_1, h_2) have been analyzed. As shown in Fig. 5, as a result of the structural and load symmetry, only a quarter of the structure has been modeled by imposing suitable symmetry conditions to the nodes on the cut planes [$u_y = 0$ on the (x, z) plane and $u_x = 0$ on the (y, z) plane]. To reproduce the realistic loading conditions of an experimental compressive test without antibuckling guides, the composite panels has been compressed by means of the applied displacement field $u_y = u_0$, $u_z = 0$ to the nodes of one panel edge while the other panel edge has been left unconstrained.

Twenty-node brick layered elements (based on the integration scheme discussed in Ref. 28), fracture interface elements, and three-dimensional node-to-node contact elements were used to model the problem. The adopted 20-node brick element mesh shown in Fig. 5 is the result of a preliminary convergence study performed with eight-node and 20-node brick layered elements. In this figure

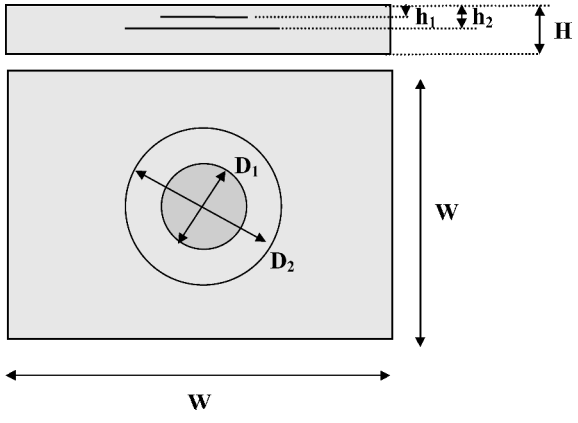

Fig. 4 Geometrical characteristics of the cross-ply laminate with embedded delaminations.

Table 1 Material property of the cross-ply laminate

Material properties (HTA/6376C)	Value
Longitudinal Young's modulus E_L, GPa	146
Transverse Young's modulus E_T, GPa	10.5
Out-of-plane Young's modulus E_Z, GPa	10.5
Poisson's ratio ν_{LT}	0.3
Poisson's ratio ν_{LZ}	0.3
Poisson's ratio ν_{TZ}	0.51
In-plane shear modulus G_{LT}, GPa	5.25
Out-of-plane shear modulus G_{LZ}, GPa	5.25
Out-of-plane shear modulus G_{TZ}, GPa	3.48
Critical ERR: mode I, J/m^2	200
Critical ERR: mode II, J/m^2	570
Ply thickness, mm	0.125

Table 2 Geometrical characteristics of cross-ply laminate

Geometrical characteristic	Value
h_1, mm	0.375
h_2, mm	1.125, 4.875
H, mm	6
D_1, mm	40, 60, 70
D_2, mm	80
W, mm	150

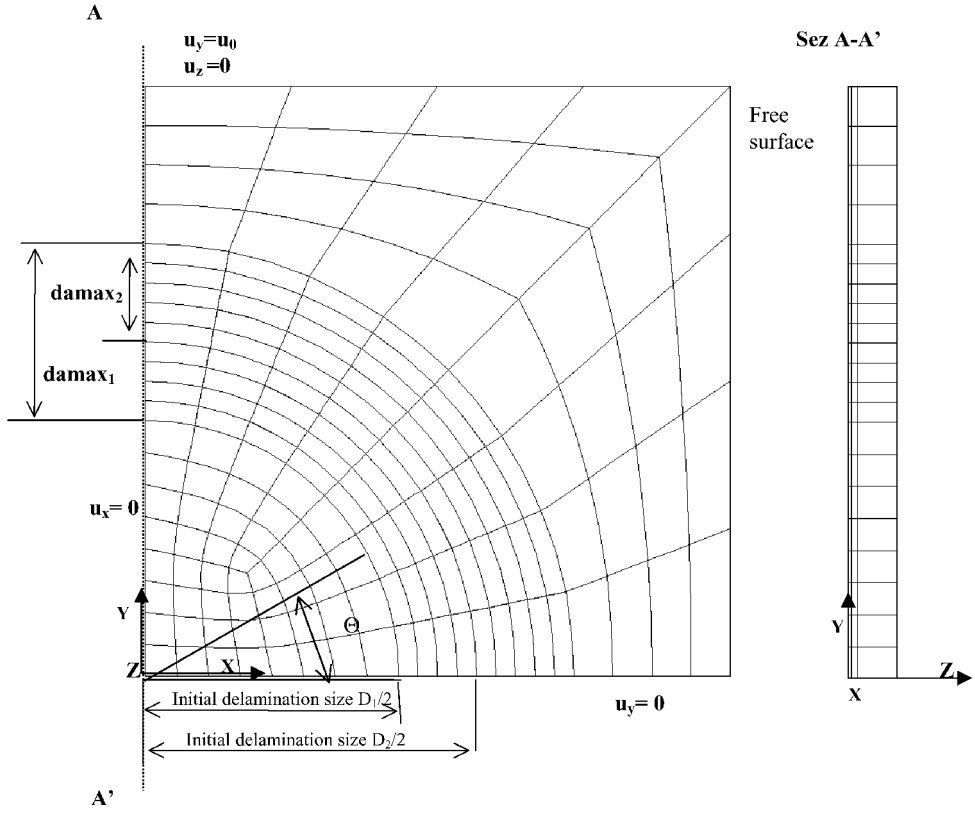

Fig. 5 Finite element mesh with applied boundary condition: in-plane view.

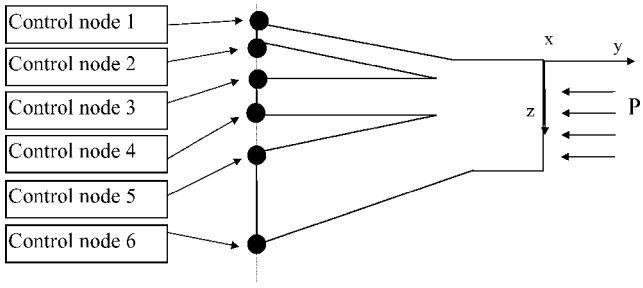

Fig. 6 Control nodes locations.

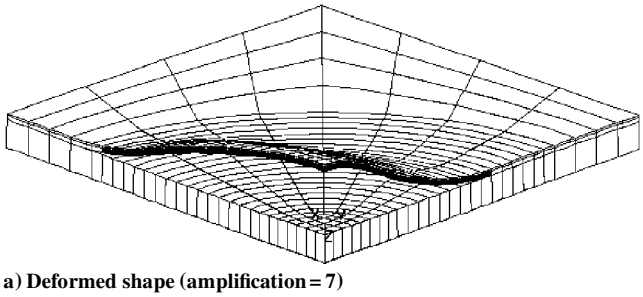

a) Deformed shape (amplification = 7)

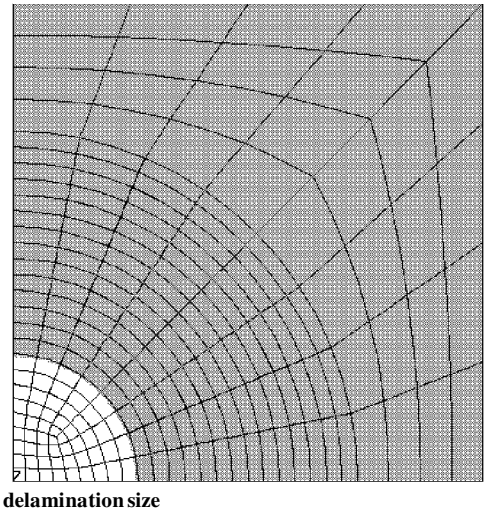

b) First delamination size

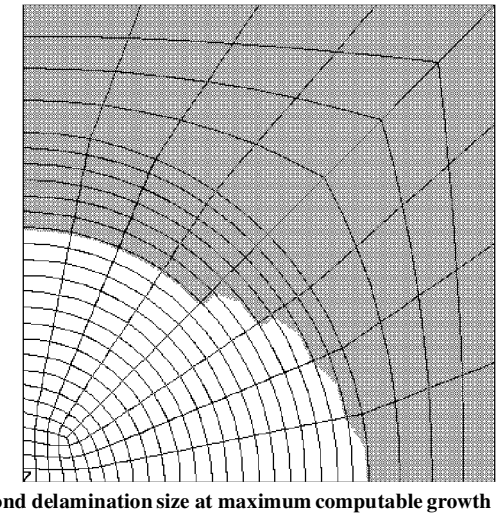

c) Second delamination size at maximum computable growth

Fig. 7 Specimen with $D1 = 40$ (mm), $D2 = 80$ (mm), $h1 = 0.375$ (mm), and $h2 = 1.125$ (mm).

the resulting model discretization in the (x, y) plane and along the thickness is clearly described. One 20-node layered brick element for each layer along the thickness has been used, and the three-dimensional material stiffness has been obtained following the integration scheme from Ref. 28.

To minimize the CPU cost, for each delamination three-dimensional node-to-node contact elements are placed between the delaminated plies in the region with $0 < \text{radius} < D_i/2$ and $0 \text{ deg} < \Theta < 90$ deg, where the rotations of the structure do not lead to significant changes in the contact normal. The interface fracture elements are placed between the delaminated plies in the region with $D_i/2 < \text{radius} < (D_i/2 + \text{damax}_i)$ and $0 \text{ deg} < \Theta < 90$ deg. They are distributed along Θ and r directions in order to monitor the energy release rate values in the neighborhood of delaminations. Thus it is possible to keep track of the delamination front changes during the growth, simply releasing the nodes where relation (2) is satisfied.

To monitor the compressive behavior of the delaminated plies, some nodes laying on the Z axis and suitably positioned along the

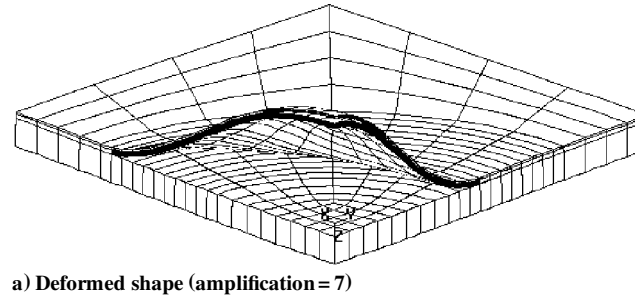

a) Deformed shape (amplification = 7)

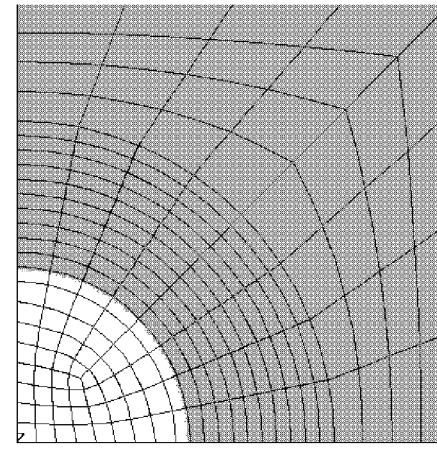

b) First delamination size

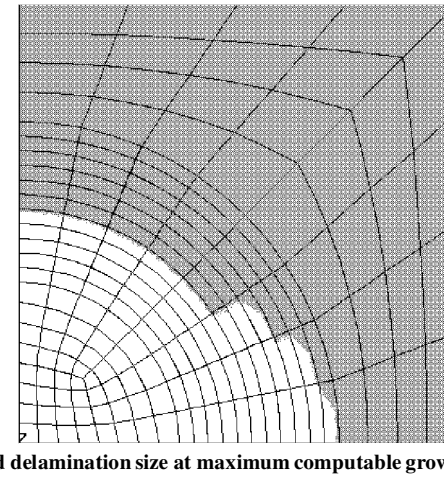

c) Second delamination size at maximum computable growth

Fig. 8 Specimen with $D1 = 60$ (mm), $D2 = 80$ (mm), $h1 = 0.375$ (mm), and $h2 = 1.125$ (mm).

panel thickness are chosen as control nodes for postprocessing purposes. In Fig. 6 the position of the control nodes of delaminated plies is schematically shown. Preliminary nonlinear numerical analysis has been performed on a finite element model of the undamaged panel in order to investigate the global buckling phenomenon without the influence of delaminations. In this preliminary computation the global buckling occurred at the load level of 110 Kn.

In Figs. 7–10 the deformed shapes (amplification factor = 7) and the growth of both the delamination for the four analyzed geometrical configurations are shown; for sake of clarity, the boundaries of buckled delaminations are marked in black. The maximum computable delamination growth depends on the number of interface fracture elements used in the model. With reference to Fig. 5, the maximum computable growth is ruled by the condition: radius of delamination $\leq (D/2 + \text{damax})$. All of the preceding figures point out the importance of contact phenomena. In the first analyzed configuration (Fig. 7) the contact between sublaminates appears to be extended almost to the entire delamination size, whereas for the geometrical configurations of Figs. 8 and 9 the contact zone is located near the delamination front. For all of the analyzed geometrical configurations, growth has been found only for the delaminations located deeper in thickness (second delamination) because of the high amount of load needed by these delaminations to reach the local buckling (Table 3). The consequent increase of tip stresses, needed to get the momentum equilibrium, leads to an increase of ERR near the delamination front. Contacts between sublaminates also influence the ERR distributions along the delaminations front, bringing down the G_I (fracture mode I) values as it can be seen from Figs. 11–14, where the G_I and G_{II} distributions along the delamination front at the growth initiation phase are shown.

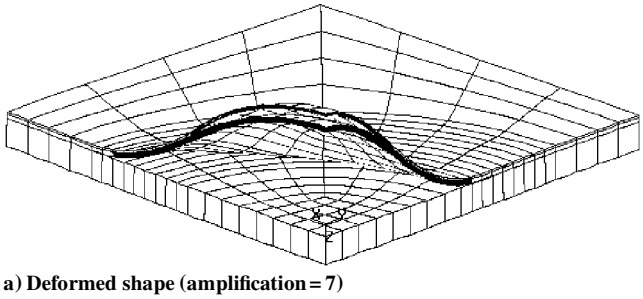

a) Deformed shape (amplification = 7)

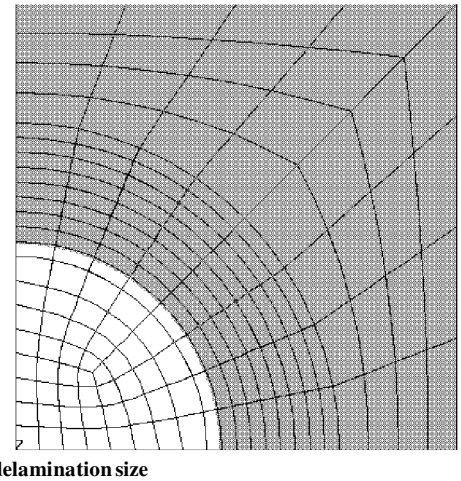

b) First delamination size

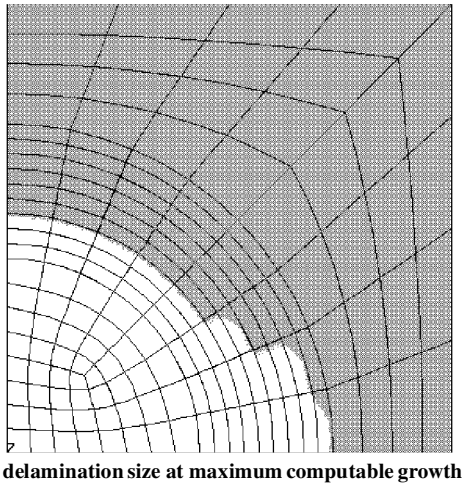

c) Second delamination size at maximum computable growth

Fig. 9 Specimen with $D1 = 70$ (mm), $D2 = 80$ (mm), $h1 = 0.375$ (mm), and $h2 = 1.125$ (mm).

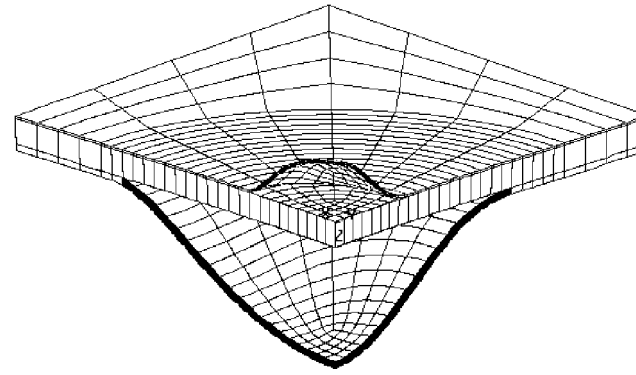

a) Deformed shape (amplification = 7)

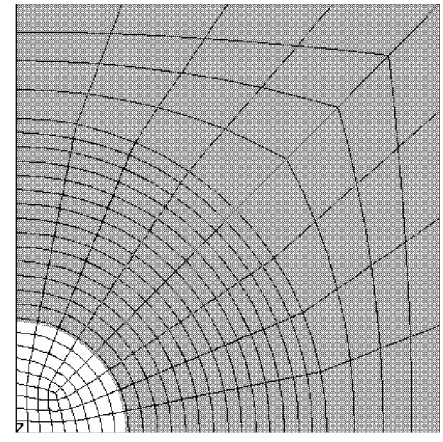

b) First delamination size

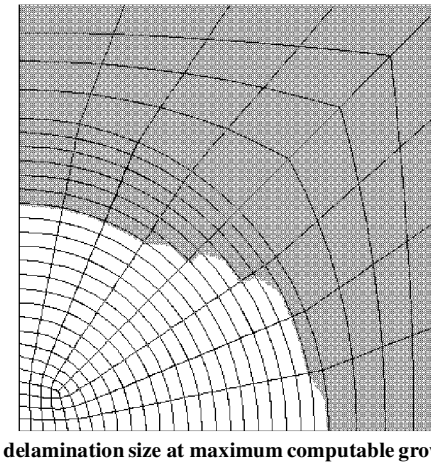

c) Second delamination size at maximum computable growth

Fig. 10 Specimen with $D1 = 40$ (mm), $D2 = 80$ (mm), $h1 = 0.375$ (mm), and $h2 = 4.875$ (mm).

Table 3 Summary of the numerical investigation

Specimen	Local buckling load, N, delamination 1	Local buckling load, N, delamination 2	Growth initiation load, N, delamination 2	Max growth load, N, delamination 2
$D1 = 40$ mm $D2 = 80$ mm $h1 = 0.375$ mm $h2 = 1.125$ mm	11,521	35,194	84,178	83,430
$D1 = 60$ mm $D2 = 80$ mm $h1 = 0.375$ mm $h2 = 1.125$ mm	6,776	25,523	68,192	67,598
$D1 = 70$ mm $D2 = 80$ mm $h1 = 0.375$ mm $h2 = 1.125$ mm	4,986	21,281	62,834	62,386
$D1 = 40$ mm $D2 = 80$ mm $h1 = 0.375$ mm $h2 = 1.125$ mm	15,973	41,767	86,154	86,154

At growth initiation the maximum ERR values should fulfill relation (2) with the condition $E_d = 1$; nevertheless, both G_{I} and G_{II} in Figs. 11 and 14 are substantially higher than in Figs. 12 and 13. This discrepancy is caused by the FEM discretization (Δa) used in the model. Ad hoc analyses have shown that, for some geometrical configurations, the delamination growth is strongly unstable[23,24] so that it should be necessary to use a very fine mesh near the delamination front to fulfill the $E_d = 1$ condition. However, the overestimation of the growth initiation, obtained by using the actual mesh, has been found not influent on the overall unstable growth simulation.

In all of the specimens (Figs. 11–14), contact phenomena caused by the orthotropy of material influence the delamination growth of second delamination bringing down the values of G_{I} for $45 \text{ deg} \leq \Theta \leq 90$ deg. This behavior is the same as the one observed for the panel with one delamination investigated in Ref. 24 (Fig. 15).

In the first three specimen (Figs. 11–13) contacts keep down the G_{I} along the whole front of the first delamination. On the contrary larger values of G_{II} were observed along the first delamination front, as a result of the extended contact area between the buckled delaminated plies. Because of its particular delaminations' positions along the thickness, the last specimen, $D1 = 40$ (mm), $D2 = 80$ (mm), $h1 = 0.375$ (mm), and $h2 = 4.875$ (mm), exhibits an independent local buckling of the two delaminations that makes them both exhibit the same behavior (Fig. 14) as the single delaminated panel of Ref. 24.

For all of the analyzed cases, the G_{III} was found insignificant if compared to G_{I} and G_{II} as in Refs. 14 and 16; hence, it is not presented. This is also the reason why the G_{IIIc} value was not given in Table 1.

As summary of the numerical investigations, in Table 3 the characteristic loads for all of the analyzed geometrical configurations are shown. The last two columns of Table 3 show also that the maximum growth load is higher than the growth initiation load; this loss of capability to sustain compressive load is typical of delaminated panels showing unstable delamination growth. Table 3 also points out the influence of the delamination size and position on the whole compressive behavior of the investigated delaminated panels.

B. Comparison Between Contact and No-Contact Approaches

To point out the importance of contact phenomena on the compressive behavior of delaminated panels and in particular on the embedded delamination growth, a comparison between a contact and no-contact approach has been carried out for the specimen with $D1 = 40$ (mm), $D2 = 80$ (mm), $h1 = 0.375$ (mm), and $h2 = 1.125$ (mm). In Fig. 16 the deformed shape and the growth of both delaminations at maximum computed growth for the no-contact approach are shown. In this figure the wide penetration zones between sublaminates are clearly visible. Comparing Fig. 16 with Fig. 7, we can have a measure of the influence of contact phenomena on our investigations.

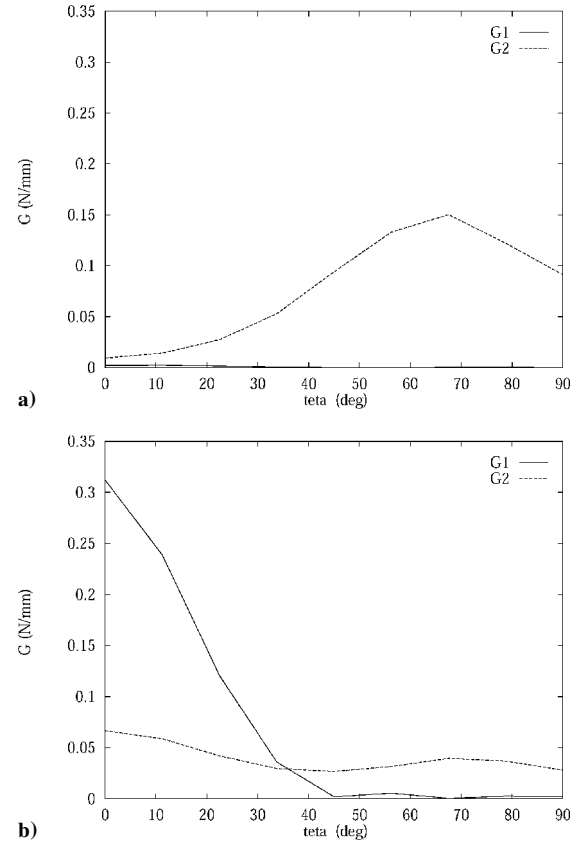

Fig. 11 ERR mode I ($G1$) and mode II ($G2$) values along the delamination front at growth initiation load for a) first delamination and b) second delamination in specimen with $D1 = 40$ (mm), $D2 = 80$ (mm), $h1 = 0.375$ (mm), and $h2 = 1.125$ (mm).

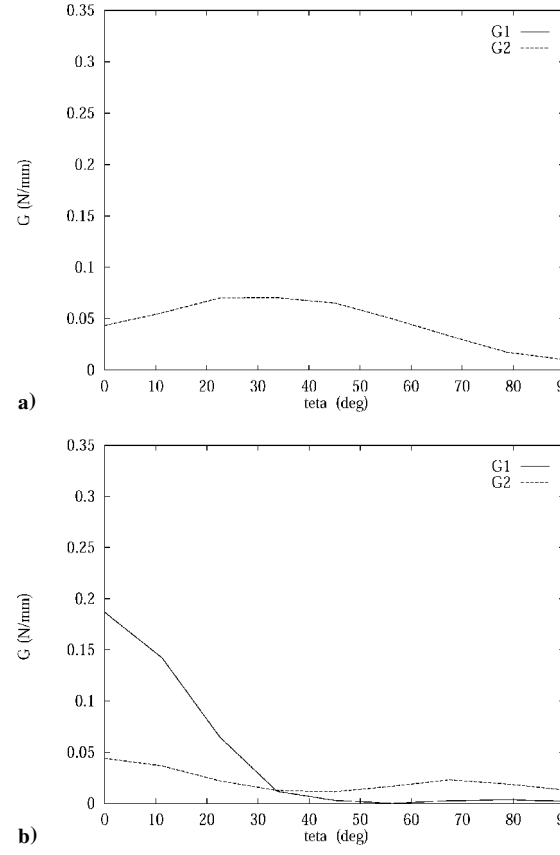

Fig. 12 ERR mode I ($G1$) and mode II ($G2$) values along the delamination front at growth initiation load for a) first delamination and b) second delamination in specimen with $D1 = 60$ (mm), $D2 = 80$ (mm), $h1 = 0.375$ (mm), and $h2 = 1.125$ (mm).

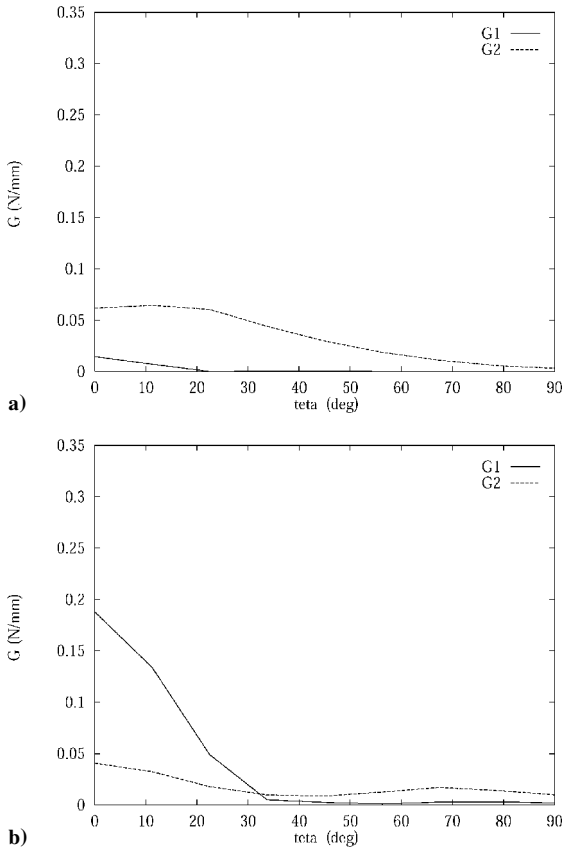

Fig. 13 ERR mode I ($G1$) and mode II ($G2$) values along the delamination front at growth initiation load for a) first delamination and b) second delamination in specimen with $D1 = 70$ (mm), $D2 = 80$ (mm), $h1 = 0.375$ (mm), and $h2 = 1.125$ (mm).

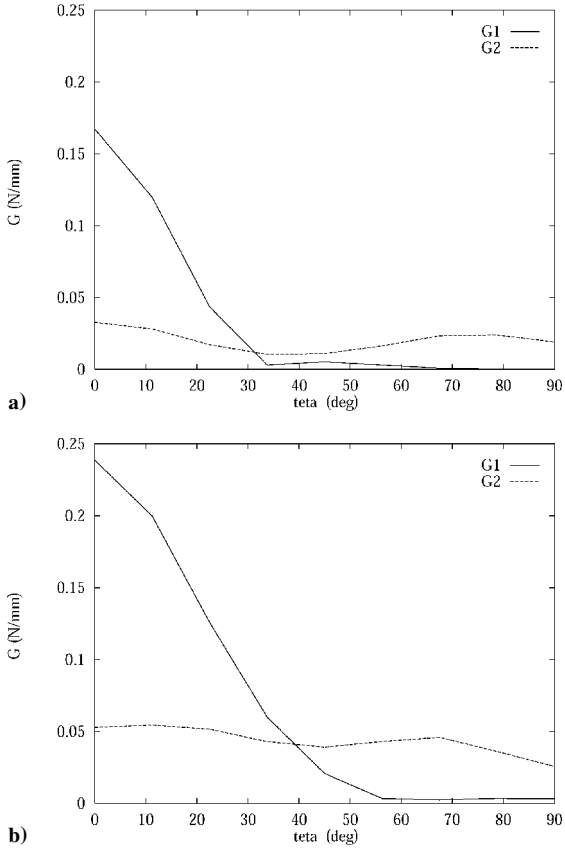

Fig. 14 ERR mode I ($G1$) and mode II ($G2$) values along the delamination front at growth initiation load for a) first delamination and b) second delamination in specimen with $D1 = 40$ (mm), $D2 = 80$ (mm), $h1 = 0.375$ (mm), and $h2 = 4.875$ (mm).

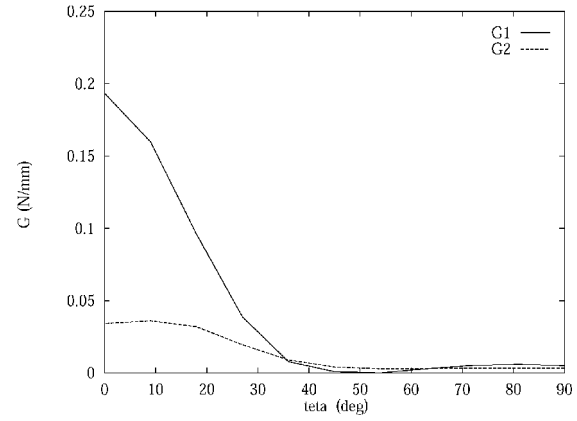

Fig. 15 ERR mode I ($G1$) and mode II ($G2$) values along the delamination front at growth initiation load in specimen with $D = 80$ (mm) and $h = 1.125$ (mm).

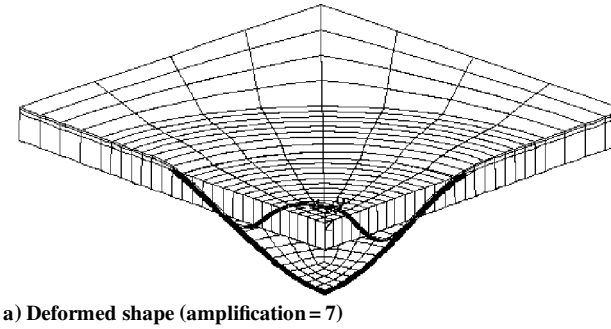

a) Deformed shape (amplification = 7)

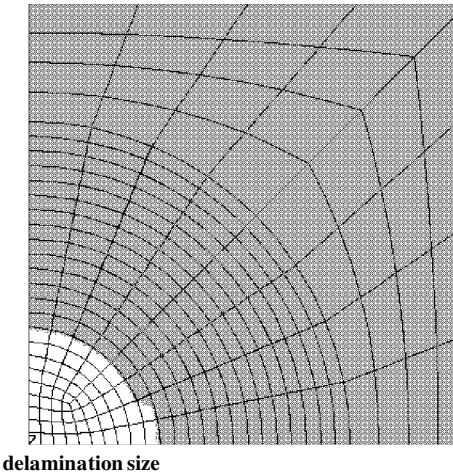

b) First delamination size

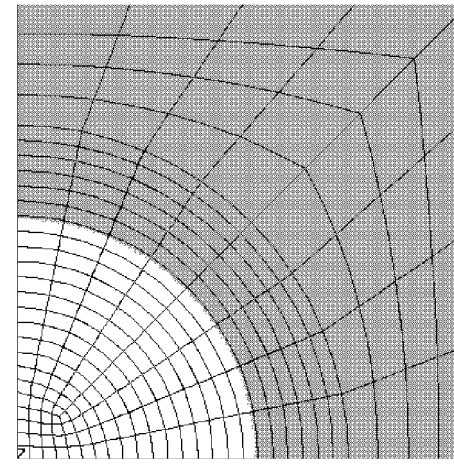

c) Second delamination size at maximum computable growth

Fig. 16 Specimen with $D1 = 40$ (mm), $D2 = 80$ (mm), $h1 = 0.375$ (mm), and $h2 = 1.125$ (mm): no-contact approach.

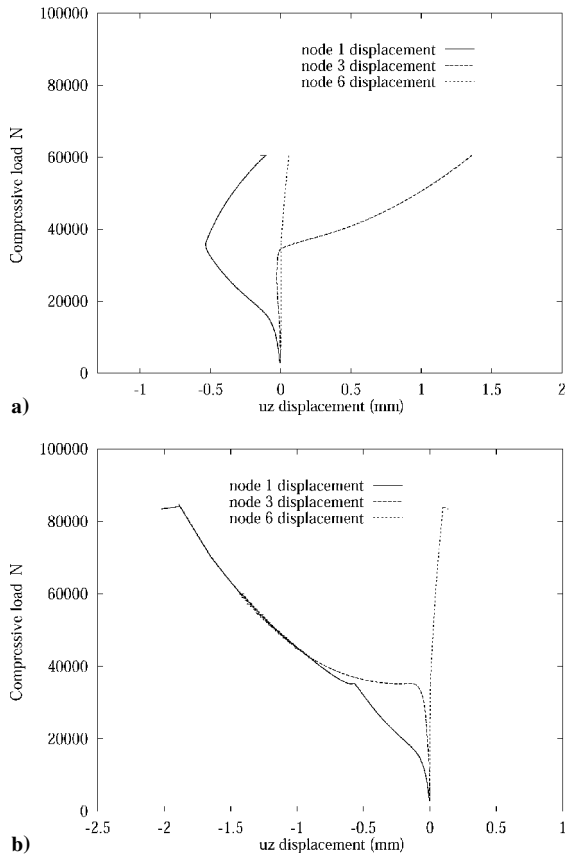

Fig. 17 Out-of-plane displacement as a function of compressive load for a) contact and b) no-contact approach in specimen with $D1 = 40$ (mm), $D2 = 80$ (mm), $h1 = 0.375$ (mm), and $h2 = 1.125$ (mm).

A measure of the penetration between plies can also be obtained from Fig. 17, where the out-of-plane displacements of the control nodes (introduced in Fig. 6), as a function of the compressive load for contact and no-contact approaches are shown.

IV. Conclusions

A numerical investigation on composite panels with two circular embedded delaminations has been presented. All of the numerical results have been found by using a nonlinear FEM code. The penalty method has been used for contact analysis, and the modified virtual crack closure technique has been used for strain energy release rate calculation. A parametric analysis has been performed to show the high influence of contact phenomena on physics of compression of composite delaminated panels. The remarkable importance of contact phenomena has been pointed out also by means of comparisons between contact and no-contact approaches.

Acknowledgments

This work is part of a cooperative agreement between the Centro Italiano Ricerche Aerospaziali, the Department of Aerospace Engineering of Seconda Università di Napoli, and the Aerospace Department of Università di Roma "La Sapienza."

References

[1]Whitcomb, J. D., "Approximate Analysis of Postbuckled Through-the-Width Delaminations," *Composite Technology Review*, Vol. 4, No. 3, 1982, pp. 71–77.

[2]Whitcomb, J. D., "Parametric Analytical Study of Instability-Related Delamination Growth," *Composite Science and Technology*, Vol. 25, No. 1, 1986, pp. 18–48.

[3]Chai, H., Babcok, C. D., and Knauss, W. G., "One Delamination Modelling of Failure in Laminated Plates by Delamination Buckling," *International Journal of Solids and Structures*, Vol. 17, No. 1, 1981, pp. 1069–1083.

[4]Ashizawa, M., "Fast Interlaminar Fracture of a Compressively Loaded Composite Containing a Defect," *Proceedings of the Fifth DOD/NASA Conference on Fibrous Composites in Structural Design*, Vol. 1, NASA, 1981, pp. 1–269.

[5]Ramkumar, R. L., "Fatigue Degradation in Compressively Loaded Composite Laminates," NASA CR-165681, 1981.

[6]Ramkumar, R. L., "Performance of a Quantitative Study of Instability-Related Delamination Growth," NASA CR-166046, 1983.

[7]Konishi, D. Y., and Johnston, W. R., "Fatigue Effects on Delaminations and Strength Degradation in Graphite-Epoxy Laminates," *Proceedings of the Composite Materials: Testing and Design (Fifth Conference)*, edited by S. W. Tsai, American Society for Testing and Materials, Philadelphia, 1979, pp. 597–619.

[8]Fei, Z., and Yin, W. L., "Postbuckling Growth of a Circular Delamination in a Laminate Under Compression and Bending," *Proceedings of the Twelfth South-Eastern Conference on Theoretical and Applied Mechanics*, 1984.

[9]Shivakumar, K. N., and Whitcomb, J. D., "Buckling of a Sublaminate in a Quasi-Isotropic Composite Laminate," *International Journal of Composite Materials*, Vol. 19, 1985, pp. 2–18.

[10]Whitcomb, J. D., and Shivakumar, K. N., "Strain-Energy Release Rate Analysis of a Laminate with a Postbuckled Delamination," *Numerical Methods in Fracture Mechanics*, NASA TM-89091, 1987.

[11]Byers, B. A., "Behaviour of Damaged Graphite/Epoxy Laminates Under Compression Loading," NASA CR-159293, 1980.

[12]Chai, H., Knauss, W. G., and Babcock, C. D., "Observation of Damage Growth in Compressively Loaded Laminates," *Journal of Experimental Mechanics*, Vol. 23, No. 3, 1983, pp. 329–337.

[13]Kim, H. J., and Hong, C. S., "Buckling and Postbuckling Behaviour of Composite Laminates with an Embedded Delamination," *Proceedings of ICCM-10*, Whistler Blackcomb, BC, Canada, 1995.

[14]Singh, K. L., Dattaguru, B., Ramamurthy, T. S., and Mangalgiri, P. D., "Delamination Tolerance Studies in Laminated Composite Panels," *Sadhana*, Vol. 25, Pt. 4, 2000, pp. 409–422.

[15]Whitcomb, J. D., "Analysis of a Laminate with a Postbuckled Embedded Delamination, Including Contact Effects," *International Journal of Composite Materials*, Vol. 26, No. 10, 1992, pp. 1523–1535.

[16]Whitcomb, J. D., "Three Dimensional Analysis of a Postbuckled Embedded Delamination," *International Journal of Composite Materials*, Vol. 23, 1989, pp. 862–889.

[17]Shahwan, K., and Waas, A. M., "Unilateral Buckling of Rectangular Plates," *International Journal of Solids and Structures*, Vol. 31, No. 1, 1994, pp. 75–89.

[18]Shahwan, K., and Waas, A. M., "Buckling of Unilaterally Constrained Plates:Application to the Study of Delaminations in Layered Structures," *Journal of the Franklin Institute*, Vol. 335B, No. 6, 1998, pp. 1009–1039.

[19]Nilsson, K.-F., Thesken, J. C., Sindelar, P., Giannakopoulos, A. E., and Storakers, B., "A Theoretical and Experimental Investigation of Buckling Induced Delamination Growth," *Journal of the Mechanics and Physics of Solids*, Vol. 41, No. 4, 1993, pp. 749–782.

[20]Shahwan, K. W., and Waas, A. M., "Non-Self-Similar Decohesion Along a Finite Interface of Unilaterally Constrained Delaminations," *Proceedings of the Royal Society of London*, Vol. 453, 1997, pp. 515–550.

[21]Perugini, P., Riccio, A., and Scaramuzzino, F., "Influence of Delamination Growth and Contact Phenomena on the Compressive Behaviour of Composite Panels," *International Journal of Composite Materials*, Vol. 33, No. 15, 1999, pp. 1433–1456.

[22]Riccio, A., Perugini, P., and Scaramuzzino, F., "Development of an Effective Numerical Tool for Predicting the Compressive Behaviour of Delaminated Composite Panels," *Advances in Computational Structural Mechanics*, Civil-Comp Press, Edinburgh, 1998, pp. 163–174.

[23]Gaudenzi, P., Perugini, P., and Riccio, A., "Post-Buckling Behaviour of Composite Panels in the Presence of Unstable Delaminations," *Composite Structures*, Vol. 51, No. 3, 2001, pp. 301–309.

[24]Riccio, A., Perugini, P., and Scaramuzzino, F., "Embedded Delamination Growth in Composite Panels Under Compressive Load," *Proceedings of ASME Conference*, American Society of Mechanical Engineers, New York, 1999; also *Composites: Part B*, Vol. 32, 2001, pp. 209–218.

[25]Merazzi, S., and de Boer, A., "B2000 Manuals," SMR Corp., Bienne, Switzerland, June 1994.

[26]Riks, E., "The Application of Newton's Method to the Problem of Elastic Stability," *Journal of Applied Mechanics*, Vol. 39, 1972, pp. 1060–1066.

[27]Tada, H., Paris, P. C., and Irwin, G. R., "Stress Analysis of Cracks Handbook," Paris Production, St. Louis, MO, 1985.

[28]Yunus, S. M., Kohnke, P. C., and Saigal, S., "An Efficient Through-Tickness Integration Scheme in a Unlimited Layer Doubly Curved Isoparametric Composite Shell Element," *International Journal for Numerical Methods in Engineering*, Vol. 28, 1989, pp. 2777–2793.

A. M. Waas
Associate Editor